Pergamon

PII: S0191–8141(97)00102–8

Journal of Structural Geology, Vol. 20, No. 5, pp. 503–516, 1998

0191-8141/98 $19.00 + 0.00

The role of bed-parallel slip in the formation of blind thrust faults

FERNANDO NIÑO

Lab. Géophysique et Tectonique, University Montpellier II, F-34095, Montpellier Cedex 05, France

and

BRGM - DR/GIG, 117 Av. Luminy—B.P. 167, 13276, Marseille Cedex 09, France

HERVÉ PHILIP and JEAN CHÉRY

Lab. Géophysique et Tectonique, University Montpellier II, F-34095, Montpellier Cedex 05, France

(*Received* 7 *March* 1997; *accepted in revised form* 21 *October* 1997)

Abstract—A finite-element code is used to model the mechanical behaviour of elastoplastic sedimentary layers that are deformed by the movement of a faulted, deformable basement. The propagation of the blind thrust fault is analysed in terms of the evolution of strain localization in the elastoplastic layers of strain-softening and strain-hardening materials. The role of layer thickness, bedding-parallel slip, and fault dip are also studied. We found that, if no interlayer slip is allowed, blind thrusts tend to propagate with constant dip, regardless of the rheological properties of the sediment layers; however, if bedding-parallel slip is present, a mechanical decoupling appears between layers, allowing stress transfers along large distances and favouring the formation of backthrusts. Fault dip also has significant influence on the qualitative behaviour; when interlayer slip is possible, a steep fault will tend to split. © 1998 Elsevier Science Ltd. All rights reserved

INTRODUCTION

The interpretation of surface folds as the expression of buried fault activity is difficult to assess. In the seismic events of El Asnam, Algeria, in 1980 (Philip and Meghraoui, 1983), and Northridge in 1994 (Yeats and Huftile, 1995), the faults were not recognized before the earthquakes took place. Some techniques have been proposed to predict subsurface geometries in terms of surface deformations, such as balanced cross-sections and fault-bend folding theory (Suppe, 1983; Woodward *et al.*, 1989), and have been used extensively to evaluate earthquake hazards (e.g. Huftile and Yeats, 1996; Shaw and Suppe, 1996). Nevertheless, forward modelling is found to be a useful tool for gaining new insights into the problem. The general interest of this approach is twofold: first, to determine under what conditions one might expect a deep thrust fault to steepen or flatten when reaching the surface; second, to find new clues for interpreting ground deformations in terms of fault geometry.

Fault propagation has been studied using a variety of techniques, such as physical (sandbox), analytical and numerical modelling. Sandbox models were first used by Sanford (1959) as a physical analogue of fault rupture propagation. The physical mechanisms that create the "faults" in the scaled model are supposed to be similar to those acting in nature. Interesting work has been done by Morse (1977a,b), trying to reproduce thrust fault propagation. Instead of using sand, Morse used rocks under 50 MPa confining pressure to mimic their behaviour at a larger scale. However, despite his efforts to lubricate the five layers of limestone used, he did not observe bed-parallel slip, the main issue discussed in the present paper. Cole and Lade (1984) and Lade *et al.* (1984) used the same approach to study the shapes and location of failure surfaces in dense and loose sand, subject to underlying dip-slip fault movement. They found that the shape of such surfaces could be described by a logarithmic spiral, defined only in terms of dip and dilation angles. Analytical models have been formulated since Hafner's classic paper (Hafner, 1951), which indicated a method to evaluate failure surfaces based on the stress state of an elastic system. Patton and Fletcher (1995) have recently obtained an analytical solution for the state of stress and deformation of an isotropic viscous or incompressible elastic layer subject to rigid-block motion at its base. The stress distribution is used as in Hafner's paper to infer the onset, distribution and nature of brittle failure. The main drawback of this approach is that results are strictly valid only for infinitesimal strain.

More recently, Bray *et al.* (1994a) studied fault rupture patterns of examples in inverse, normal and strike-slip faults. They emphasized the importance of the rheological characteristics of the soil (of thickness $\sim$100 m; as opposed to 4 km which could be considered a typical thickness of sedimentary sequences) overlying the bedrock fault on its rupture propagation pattern. In their subsequent paper Bray *et al.* (1994b), used the finite-element method to model the fault-propagation properties of cohesive soils, concentrating in reproducing their non-linear behaviour by using Duncan's hyperbolic stress–strain model (Duncan *et al.*, 1980). They presented their work under the assumption that the strength of soils is not significantly reduced after failure, and that pre-failure character-

istics of the stress–strain curve were the most important factors to be considered. Their simulation involved transforming the rheological properties of the elements during deformation in order to simulate post-peak behaviour (assigning a very low elastic modulus to represent a no-tension element). The results were presented as stress-levels and tension/shear failure levels; however, this numerical technique did not take into account either softening properties of the soil or the possibility of relative slip between soil layers because of the limited thickness of the soil layer. Other numerical simulations (i.e. Lebel and Mountjoy, 1995) are the implementation of empirical laws (like that of Walsh and Watterson, 1988). Caskey (1995) deduced some geometrical relations in dip-slip faults that enabled him to establish new nomograms for estimating fault displacement in the field. However, this approach does not consider the shape of the failure path. Roering *et al*. (1997) used the boundary element method to study the fracture of an elastic layer above a fault plane. Their analysis is based on the evaluation of the stress-intensity factors of fracture mechanics (Lawn, 1993) but is restricted to linear elasticity and isotropic, homogeneous materials. The likelihood of propagation of the fault is calculated (via the stress-intensity factors), but not their propagation path.

All techniques which address the problem of fault propagation can be classified either as rigid block or deformable basement models. The rigid-block hypothesis considers that the basement, when compared with the overlying sediments, is so competent that its deformation can be neglected. The deformable basement models relax this constraint and can hence be applied to low-contrast basement/sediment rheologies. To our knowledge, only the photoelastic model of Rodgers and Rizer (1981) considers the case of a deformable basement. This study disregards most of the more or less unrealistic hypotheses of the models hitherto described. We use a numerical approach for analysing the mechanical behaviour of elastoplastic sedimentary layers subject to large strain, with appropriate physical scaling. Both rigid and deformable blocks may be used to model the faulted basement, the model being valid for low- and high-contrast rheologies. Additionally, bed-parallel slip effects are taken into consideration as a way of analysing the contributions of folding and faulting to absorbing deformation.

STRAIN LOCALIZATION IN CONTINUA

In experimental tests of rock deformation in the brittle field, a sample rarely undergoes homogeneous deformation. Rather than being uniform, deformation concentrates in a narrow zone, where the rock is weaker (usually as the result of heterogeneities of some kind) and where it will ultimately fail. Rudnicki and Rice (1975) established the framework within which this phenomenon could be understood when using elastic–plastic constitutive laws. The problem of formation of fault zones can then be described in terms of strain localization in an elastoplastic medium, which is the approach that will be used in this paper.

NUMERICAL METHOD

We have used a two-dimensional finite-element code to solve large strain geodynamical problems with viscous and elastoplastic rheologies under quasi-static conditions. The technique corresponds to a Lagrangian description of the geological medium and is derived from the program *FLAC* developed by Cundall (Board, 1989; Cundall, 1989). We use quadrilateral elements formed by assembling pairs of triangular elements of constant strain, while using an adaptive remeshing method (Hassani, 1994; Niño, 1997) to accurately follow strain localization phenomena. Faults are identified as regions in which intense strain localization has occurred.

SEDIMENT AND BASEMENT RHEOLOGIES

Sediment layers at the surface of the Earth are subject to relatively low pressures and temperatures. However, during their diagenesis, they have undergone many pressure–temperature regimes that, in conjunction with their granulometric and mineralogic properties, determine their present response to deformation. Experimental data on sedimentary rocks show they behave either as strain-hardening or as strain-softening elastic–plastic materials (Handin and Hager, 1957; Baidyuk, 1967; Touloukian *et al*., 1981). The Drucker–Prager law presented in the Appendix, can model the main features of strain-softening and strain-hardening materials; namely a dependence on pressure and deviatoric stress. The strain-softening/hardening parameter used in this model depends both on the internal friction angle (itself a function of strain) and on the dilatancy angle (which we will assume to be zero in all our models).

Shales, limestones and sandstones are the predominant sedimentary rocks in the Earth's crust (Meissner, 1986). Muddy shale, and Darley Dale sandstone are examples of strain-softening sedimentary rocks; Wolfcamp limestone and Repetto siltstone are examples of strain-hardening sedimentary rocks. The stress–strain curves of these sedimentary rocks are shown in Fig. 1, where experimental data is superposed on the curve reproduced by using Drucker–Prager's constitutive law.

The rheology of the basement will be assumed to be elastic–plastic (Drucker–Prager) with parameters similar to those of granite: Young's modulus of $E = 10^{11}$ Pa, Poisson's ratio of $v = 0.25$, density of $\rho = 2700$

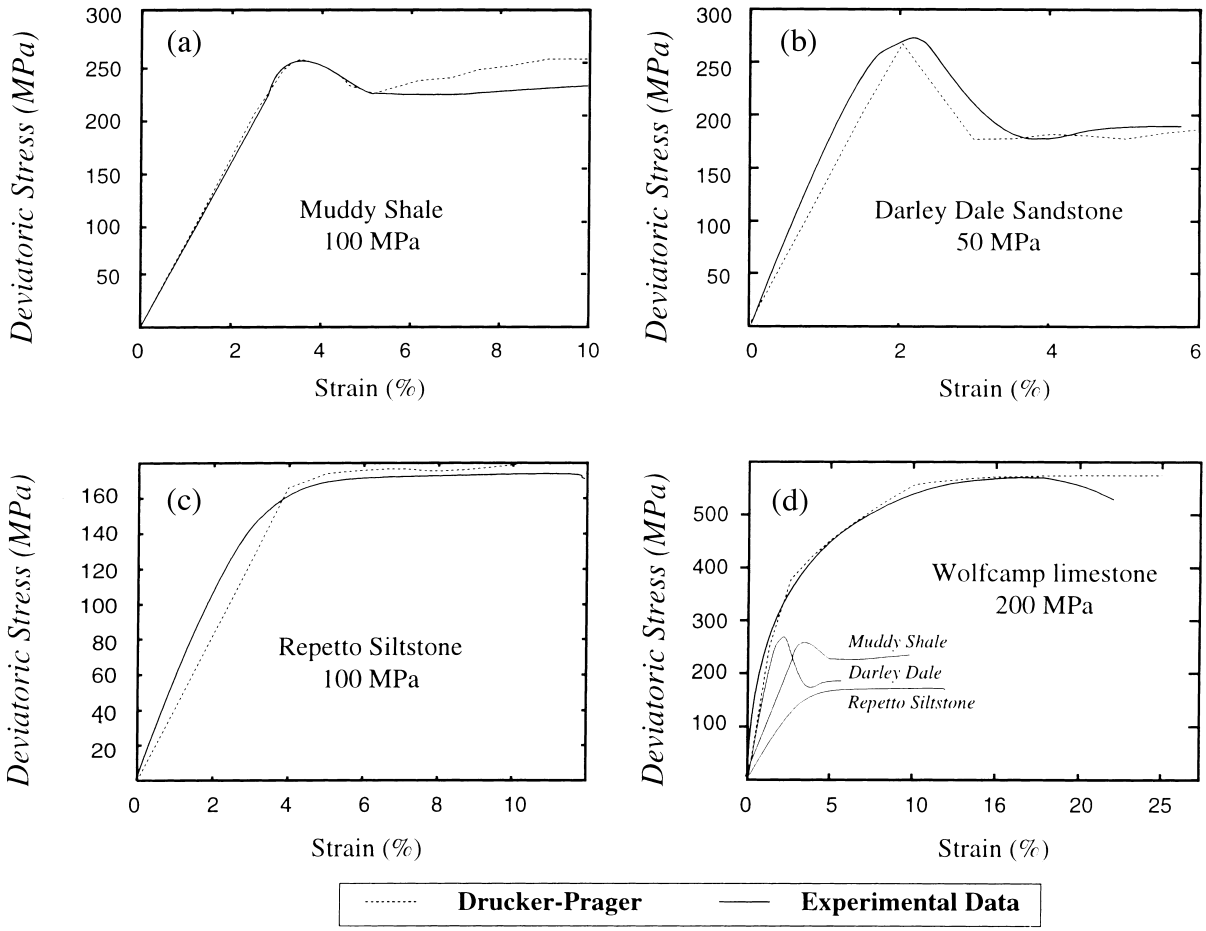

Fig. 1. Stress–strain curves for strain-softening sedimentary rocks. All data are from triaxial compression tests at ambient temperature; the confining pressures are written under the name of the studied rock. Experimental data are shown with a continuous line, the curve reproduced by the Drucker–Prager model being the dotted line. (a) Strain-softening Muddy shale (Baidyuk, 1967; Handin and Hager, 1957). (b) Strain-softening Darley-Dale sandstone (Baidyuk, 1967; Handin and Hager, 1957). (c) Strain-hardening Repetto siltstone (Handin and Hager, 1957; Johnson, 1980). (d) Strain-hardening Wolfcamp limestone (Handin and Hager, 1957; Johnson, 1980); the experimental data of samples (a)–(c) are reproduced in (d) for comparison.

kg/m^3, constant internal friction angle of $\phi = 30^\circ$ and no dilatancy.

MECHANICAL MODELS

The experiments that will be discussed are all based on variations of the standard mechanical model shown in Fig. 2. This model considers three kinds of rheologies. The uppermost layers represent the sedimentary cover where fault propagation is to be studied. Bed-parallel slip between these layers is permitted in selected experiments (with a very low friction coefficient $\mu = 0.05$). The second kind of rheology is that of the faulted basement which is welded to the deepest sedimentary layer. This rheology will be kept fixed as described in the previous section. The fault tip does not terminate at the sediment–basement interface, but for numerical reasons (avoiding triple points), is artificially prolongated to half the thickness of the deepest sedimentary layer. Two additional conditions are included to facilitate numerical modelling: fault slip is negligible at the base of the model, and the geological system evolves in isostatic conditions. In order to meet these conditions, the fault plane is extended downward through a viscous layer (the third rheology used: linear viscosity) that absorbs fault slip at depth. A hydrostatic pressure is applied at the base of the model so as to provide isostatic equilibrium. The overall dimensions of the model are 30 km wide and 10 km deep. We impose an overall shortening rate of 1 cm/y for a period of 100,000 y; i.e. a total shortening of 1 km. The geological problem we address is expressed only in the upper half of the model. Spatial discretization is undertaken by an homogeneous initial mesh of 1727 quadrilateral elements. The adaptive remeshing method enables our model to follow strain-localization phenomena increasing the number of elements to over 2500 (Fig. 3).

Effects of rheological contrast and bed-parallel slip

It is widely accepted that weak layers can give rise to décollements in the Earth's crust. In order to quan-

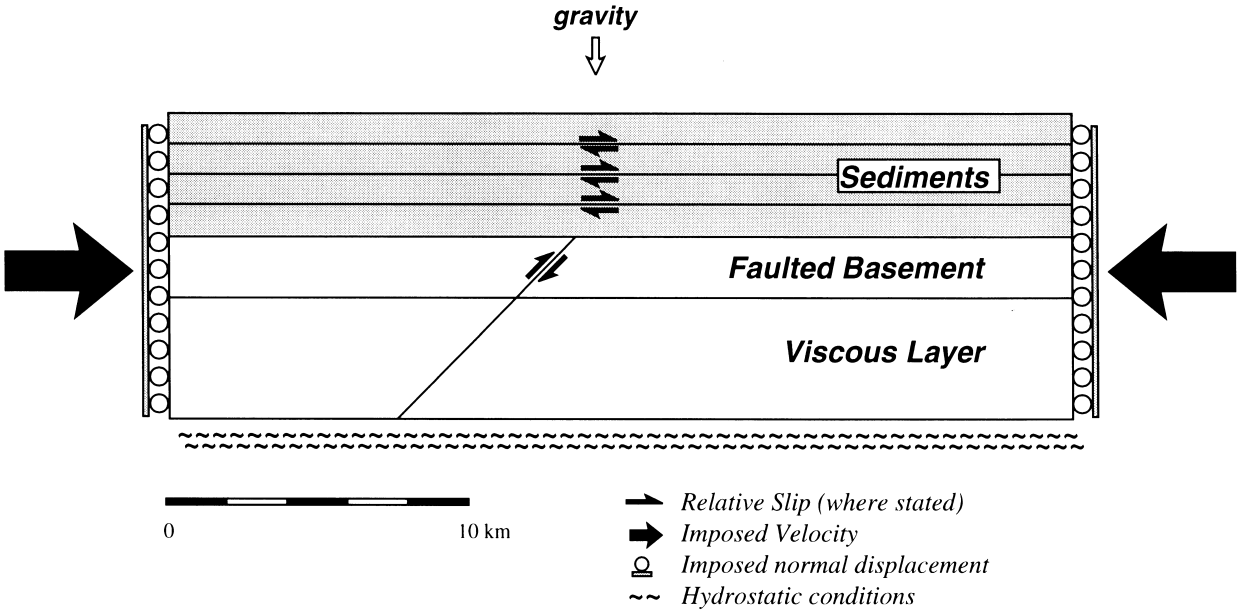

Fig. 2. The mechanical model used in these experiments. The viscous layer is introduced as a numerical convenience to hinder fault slip at depth. Hydrostatic conditions are applied at the base. The fault tip ends in the middle of the deepest sedimentary layer.

tify how weak these layers should be to significantly change the propagation path of a buried thrust fault, we have undertaken a series of experiments with different rheological contrasts while allowing no bed-parallel slip between layers, and repeated them with a very low friction coefficient ($\mu = 0.05$) between sedimentary layers. A summary of the rocks that were used in each experiment is shown in Table 1. In this case, four layers of sedimentary rocks overlie the faulted basement, the thickness of the basement being 2 km and that of each layer, 1 km. The results are shown in Fig. 4, where we plot the intensity of the deviatoric strain tensor.

It is obvious that in the case of no bed-parallel slip, the propagation path of the thrust fault, i.e. the geometry of the localization deformation zone, is just the extension of the fault plane with a constant dip. This behaviour is exhibited by all tested rheologies. The same observation holds, whatever the dip angle of the fault; this effect is clear and will not be explored further.

The case of bed-parallel slip is, by contrast, very interesting. The main fact is that a backthrust appears solely as a consequence of bed-parallel slip. The effect is most marked for the case 6 BPS, because it is constituted of Darley Dale sandstone, the most "softenable" of all materials tested (i.e. the difference between peak stress and average post-peak stress is greatest for this material—Fig. 1b). A second important observation is that the propagation path of the thrust fault is no longer straight but curves upward (case 5 BPS, particularly), giving rise to a high-angle fault at the surface. This effect is present for virtually all rheologies tested, the only difference being the intensity of deformation localization (greatest in strain-softening materials). However, above a certain degree of strain, all fault trajectories are straight in all models.

We interpret this effect as being the consequence of the mechanical decoupling of sedimentary layers. This effect is best understood by comparing side by side two cases of thrust fault formation with and without bed-parallel slip. Figure 5 shows a sequence of snapshots of deformation of the region above the fault tip at 15%, 25% and 35% of total time, for the case of four sedimentary layers with the rheology of Darley Dale sandstone. Both deviatoric stresses (with its maxi-

Table 1. Summary of the rheologies used in the experiments shown in Fig. 4

Case	Basement	Layer 1	Layer 2	Layer 3	Layer 4
1	Granitic	Muddy shale	Muddy shale	Darley D. Sst	Darley D. Sst
2	Granitic	Muddy shale	Darley D. Sst	Muddy Shale	Darley D. Sst
3	Granitic	Wolfcamp Lst	Wolfcamp Lst	Wolfcamp Lst	Wolfcamp Lst
4	Granitic	Wolfcamp Lst	Wolfcamp Lst	Darley D. Sst	Darley D. Sst
5	Granitic	Wolfcamp Lst	Repetto Siltst	Repetto Siltst	Darley D. Sst
6	Granitic	Darley D. Sst	Darley D. Sst	Darley D. Sst	Darley D. Sst
7	Granitic	Granitic	Granitic	Granitic	Granitic

Abbreviations used: Sst: Sandstone; Lst: Limestone: Siltst: Siltstone.
Layer 1 is the deepest and layer 4 the shallowest one.

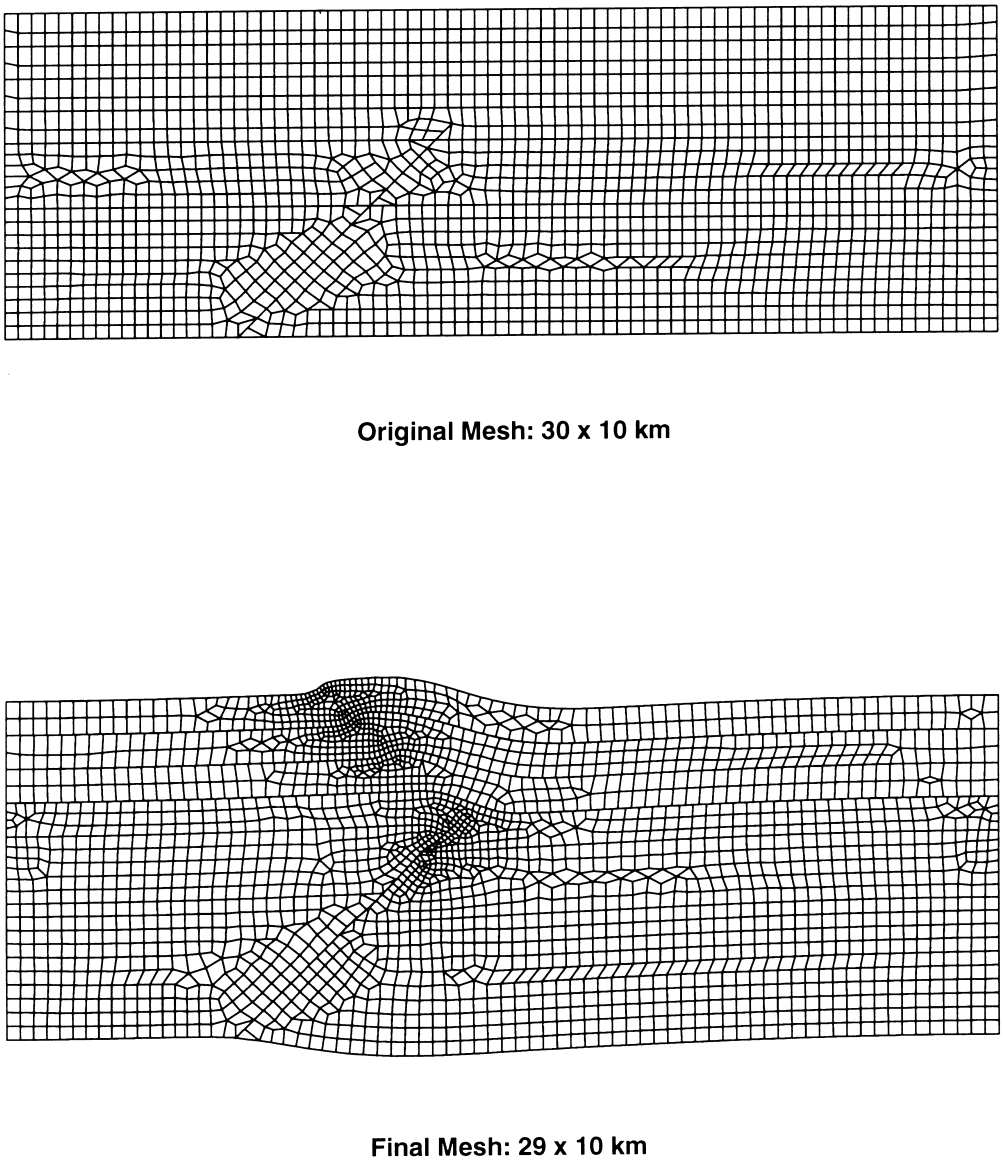

Fig. 3. Spatial discretization of case 6 BPS, at the initial stage (1727 elements) and after 1 km shortening (2632 elements). Mesh refinement follows strain-localization zones.

mum and minimum principal directions) and deviatoric strain (with the displacement field) are shown. The case where no bed-parallel slip is allowed (Fig. 5a–f), shows a continuous upward displacement field on the hanging wall, and stress is transferred freely throughout boundaries. In contrast to this behaviour, the case where bed-parallel slip is allowed shows that the slipping surfaces induce the maximum principal direction of stress to be perpendicular to the bed, thus acting as a "transfer guide" for stress whose concentration is spread over a wider surface than in the other case. As seen in (Fig. 5i & l, to be compared to Fig. 5c & f), the stress-transfer mechanism activated by the mechanical decoupling is responsible for the accumulation of stress at the left-hand side of the fault tip, thus creating the backthrusts of Figs 4 and 5i. At the same time, this effect is responsible for the change in dip of the "direct" thrust fault (compare Fig. 5c & i), which favours a steeper fault. Another way at looking at this effect is that the thrust fault creates a kink in the sedimentary layers, along which slip takes place. This movement is accommodated by straining the material on the kink plane and its prolongation, i.e. the backthrust zone. The topographical profile (Fig. 6) also shows folding is magnified by a factor of two, as a consequence of bed-parallel slip.

Effects of fault dip

Once we have accepted bed-parallel slip has a major influence on blind thrust propagation, we can consider what the effect is of changing the fault dip in our models. We will explore this effect by using models whose sedimentary layers are made of purely strain-hardening materials, purely strain-softening material,

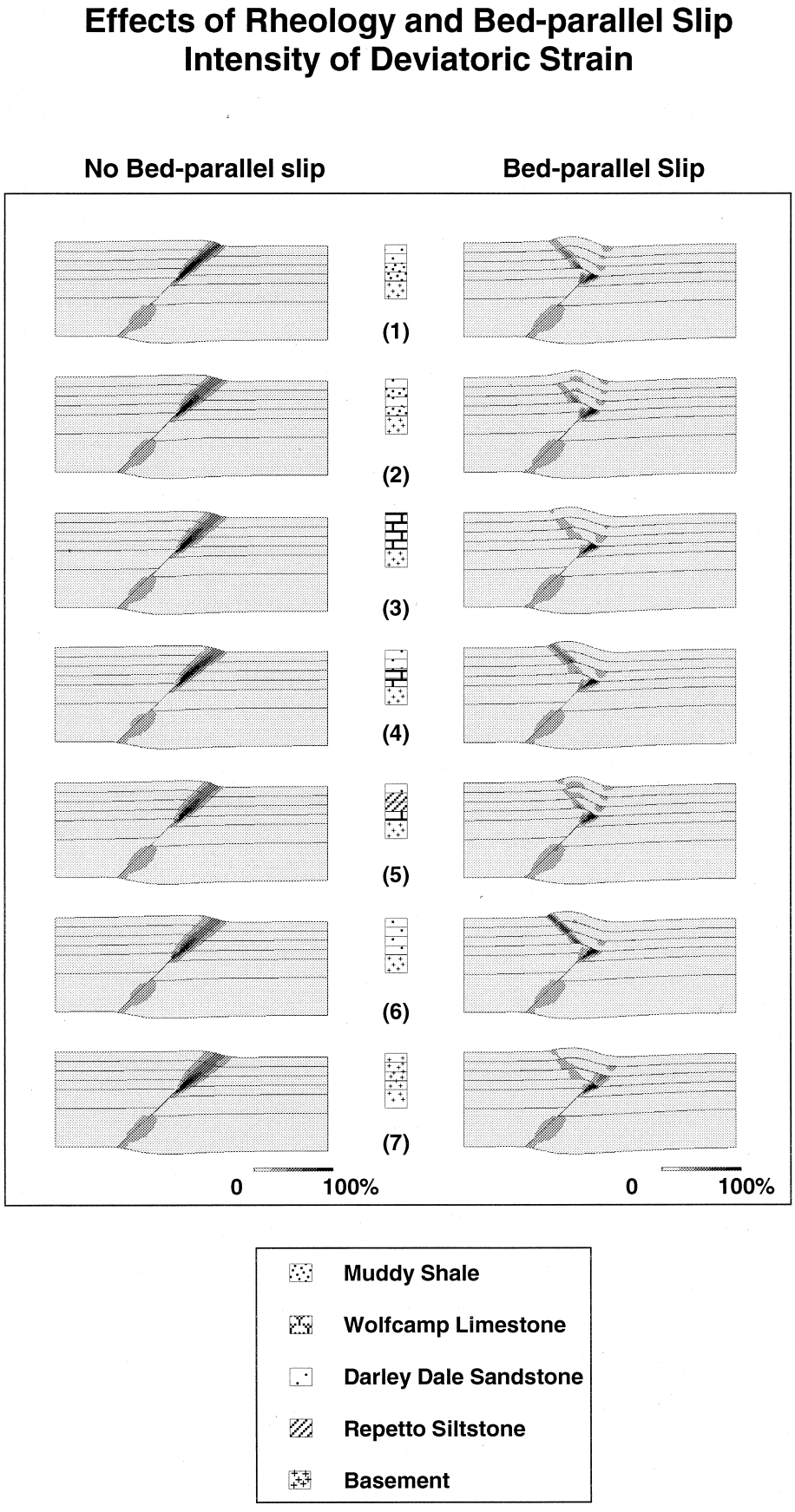

Fig. 4. The effects of rheology and bed-parallel slip for a variety of rheologies. Cases with the index BPS refer to models allowing bed-parallel slip. The gray scale shows the intensity of deviatoric strain. The zones with intense strain localization are identified as the zones of fault propagation.

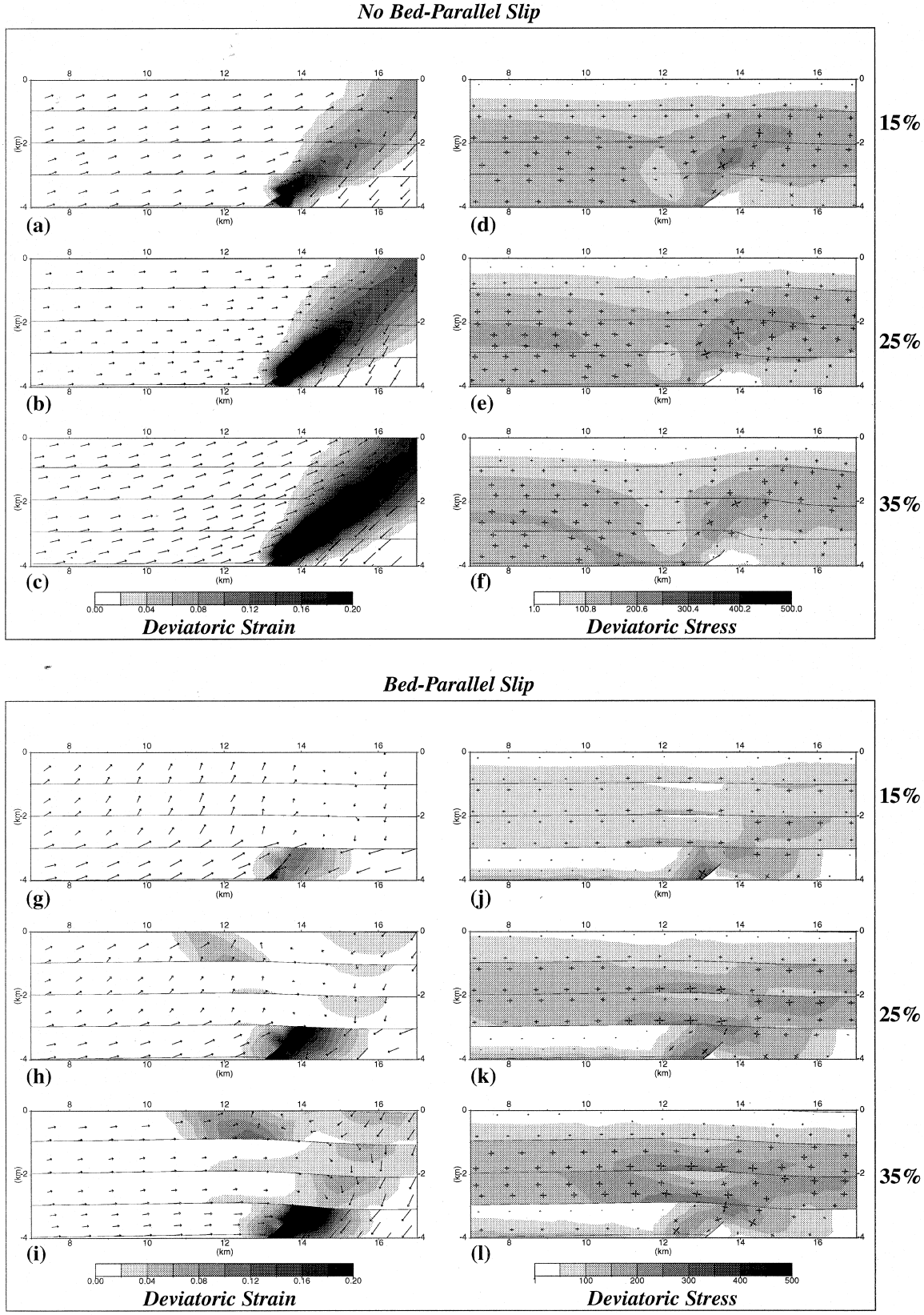

Fig. 5. Snapshots of the evolution of the deviatoric strain and deviatoric stress corresponding to cases 6 and 6 BPS. The region is the zone above the fault tip, limited between kilometres 7 and 15 (horizontally) and cover the first 4 km of sediments. The column of the left shows the intensity of deviatoric strain (as in Fig. 4) and the displacement field. The column at the right shows the intensity of deviatoric stress and the orientations of the maximum and minimum principal stresses. Snapshots correspond to 15%, 25% and 35% of the total time. See text for further details.

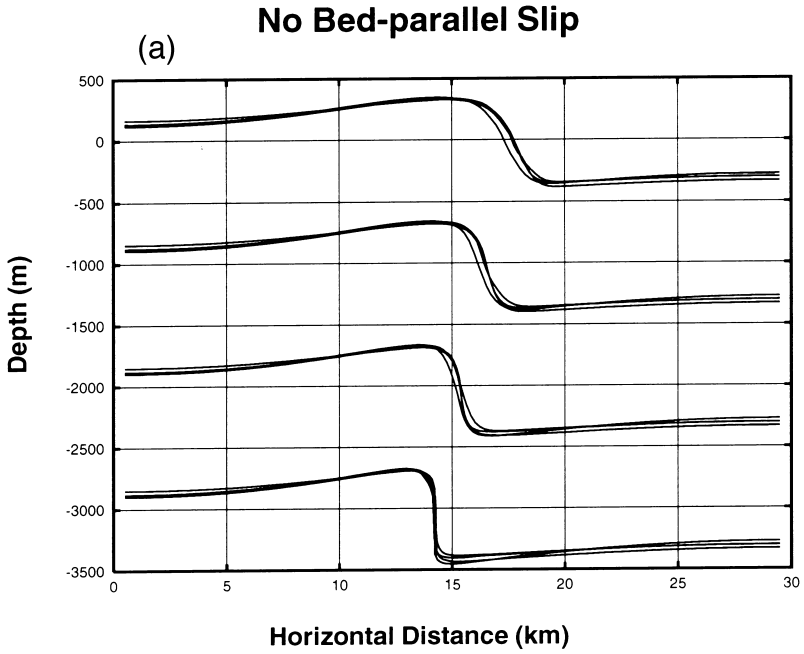

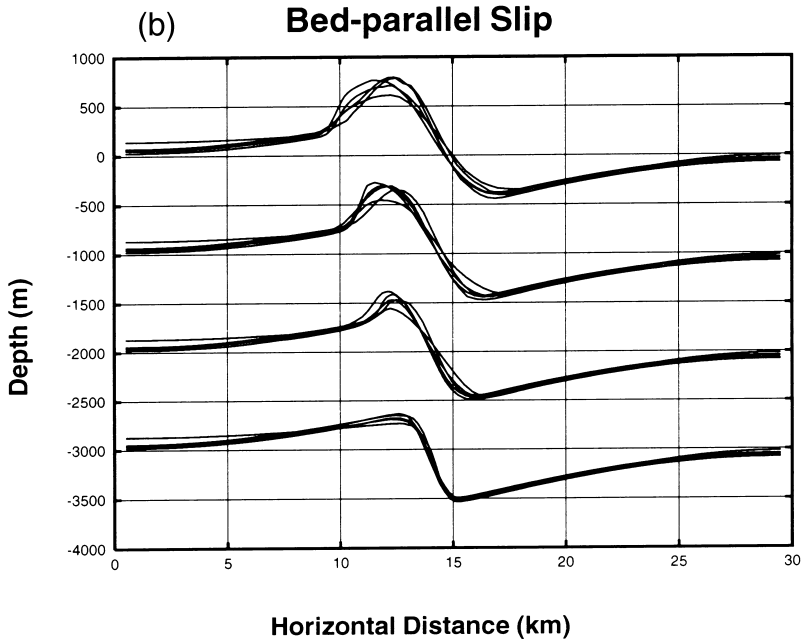

Fig. 6. Topographic profiles of the surface and of intermediate layers in cases of Fig. 4. The overall shape being the same, curves are not discriminated; the essential feature is the amplification of the folding mechanism seen in (b).

or a combination of both. A summary of the cases treated is shown in Table 2.

In Fig. 7 it is clear the backthrust effect prevails among low- and mid-angle thrust faults. However, for high-angle faults, the strain localization zone is split in two separate paths, an effect which is most evident with strain-softening materials (case 16).

The explanation to the fault splitting is easily seen if we consider how layers slip over the fault tip. Initially, the first interface where slip is allowed is just on top of the fault tip, and it is initially weakened. However, as folding progresses, the layers slip to the right of the fault tip, and previously undeformed material absorbs deformation; because of the stress-transfer mechanism cited above, it is all the small region to the left of the fault tip that becomes deformed. Eventually, the material is so weak that a parallel zone of deformation localization is formed.

Table 2. Summary of the rheologies used in the experiments shown in Fig. 7

Case	Dip	Layer 1	Layer 2	Layer 3	Layer 4
8	30°	Wolfcamp Lst	Wolfcamp Lst	Wolfcamp Lst	Wolfcamp Lst
9	30°	Wolfcamp Lst	Wolfcamp Lst	Darley D. Sst	Darley D. Sst
10	30°	Darley D. Sst	Darley D. Sst	Darley D. Sst	Darley D. Sst
11	45°	Wolfcamp Lst	Wolfcamp Lst	Wolfcamp Lst	Wolfcamp Lst
12	45°	Wolfcamp Lst	Wolfcamp Lst	Darley D. Sst	Darley D. Sst
13	45°	Darley D. Sst	Darley D. Sst	Darley D. Sst	Darley D. Sst
14	60°	Wolfcamp Lst	Wolfcamp Lst	Wolfcamp Lst	Wolfcamp Lst
15	60°	Wolfcamp Lst	Wolfcamp Lst	Darley D. Sst	Darley D. Sst
16	60°	Darley D. Sst	Darley D. Sst	Darley D. Sst	Darley D. Sst

Abbreviations as in Table 1. The basement is taken to be granitic in all cases.

Effect of layer thickness

As before, we will take the extreme cases of only strain-hardening, and only strain-softening materials. The total thickness of the sedimentary layers is held constant (i.e. 4 km), but the thickness of each individual layer is changed. A summary of the cases treated is shown in Table 3.

By changing the layer thickness is each sedimentary layer, we are limiting the bed-parallel slip mechanism. In these experiments, two competing effects become apparent. The first is that, when the number of slipping layers is reduced, the backthrust effect is diminished too (Fig. 8, case 17 and 20, almost straight propagation paths). Increasing the number of layers activates the mechanical decoupling between layers, an effect exacerbated when using seven layers. However, when the number of layers is increased, a second mechanism plays an important role in the blind thrust propagation, namely the competing effects of faulting vs folding. In Fig. 8, cases 19 and 22 we have plotted relative slip for layers at 1, 2 and 3 km deep (except for cases 17–18 where only two layers are available). It is clear that the amount of total relative slip increases as the number of layers increases; this is implicit for the plot of cases 19 and 22 (seven layers), where amplitudes of relative slip are comparable to cases 18 and 21, but the number of layers accommodating that slip is more than two times greater. Hence, deformation is rather absorbed by folding than by faulting, so shortening has to be much more important for the backthrusts to attain the same intensity as the cases with a reduced number of layers.

FIELD EXAMPLE

The Palmyrides belt, in the Arabian plate, is a representative example of intracontinental belt. This relatively narrow belt (~50 km), extends along a NE–SW direction over a distance of about 400 km, and is thought to be a result of tectonic inversion. It seems that during the Permo-Trias a NE–SW graben was formed beneath the present day location of the Palmyrides belt (O'Keefe and Sengor, 1988; May, 1991). This extensional phase ended in the late Jurassic. A second extensional phase, contemporary with the opening of the Mesogea, created important sedimentary deposits in the same zone. A compressive tectonic regime at the end of the Cretaceous initialized structural inversion. Subsequent enhancement of this inversion began during the Miocene and has continued to the present day. Cross-sections made by Salel (1993) show explicitly the consequences of tectonic inversion and fault propagation. The inverted normal fault of the Jabal Mquebra (Fig. 9), shows the existence of a backthrust that seems to be due to the active décollement between the Mulussa (evaporites) and Judea (dolomites) formations. There is evidence of significant bed-parallel slip in this case, an observation that supports the conclusions obtained from our modelling.

CONCLUSIONS

We have studied some of the parameters that may condition the propagation of a blind-thrust in sedimentary layers by using a numerical model of large strain in two-dimensions, that enables us to follow strain-localization zones. Three main hypotheses have

Table 3. Summary of the rheologies used in the experiments shown in Fig. 8

Experiment	Number of Layers	Rheology of Layers	Layer Thickness
17	3	Wolfcamp Lst	1.3 km
18	3	Darley D. Sst	1.3 km
19	4	Wolfcamp Lst	1 km
20	4	Darley D. Sst	1 km
21	7	Wolfcamp Lst	500 m
22	7	Darley D. Sst	500 m

Abbreviations as in Table 1. The basement is taken to be granitic in all cases.

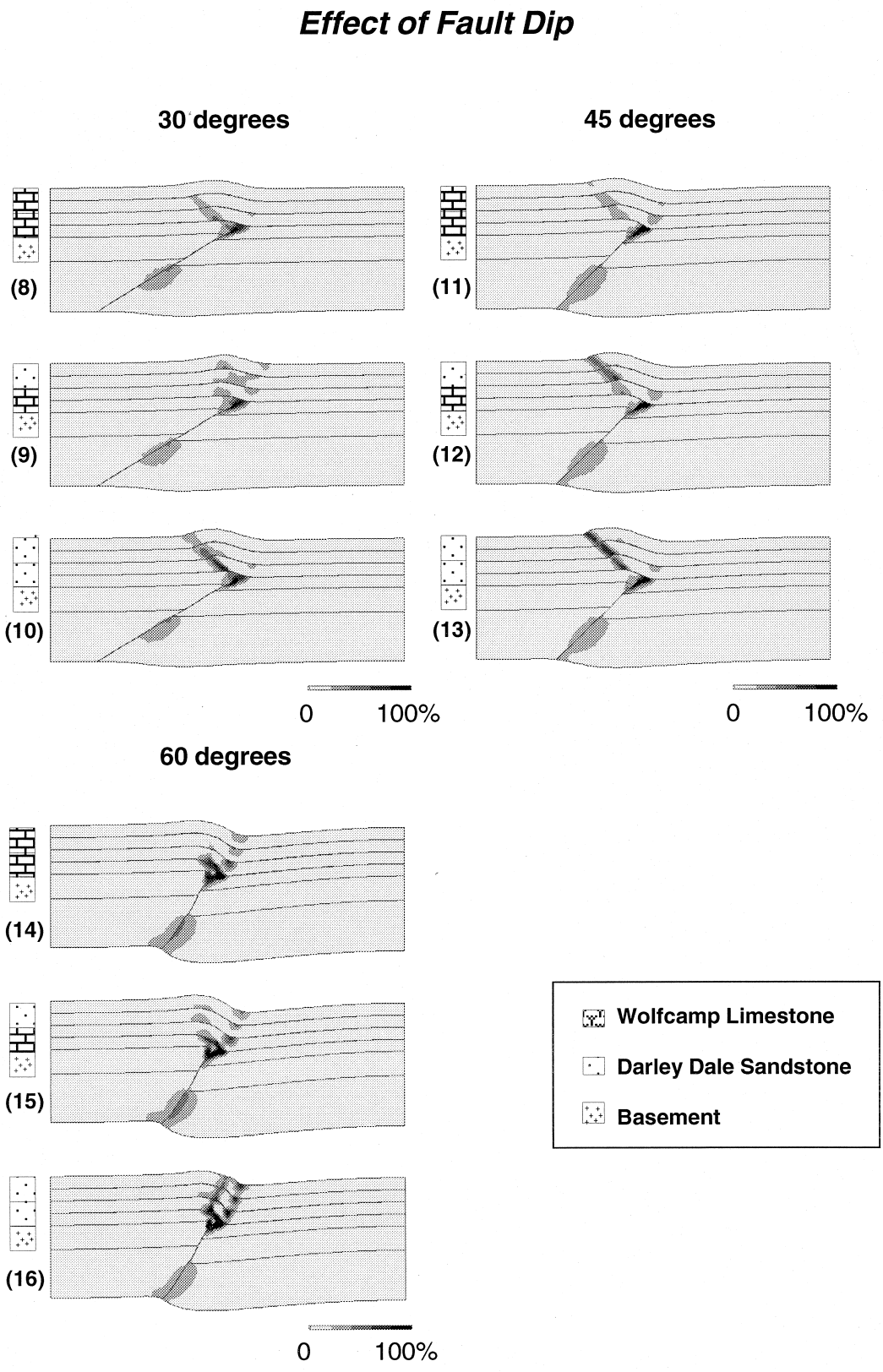

Fig. 7. Effect of fault dip on blind thrust propagation. Bed-parallel slip is allowed for strain-hardening, strain-hardening/softening and strain-softening rheologies. Case 16 is the best example of fault path splitting.

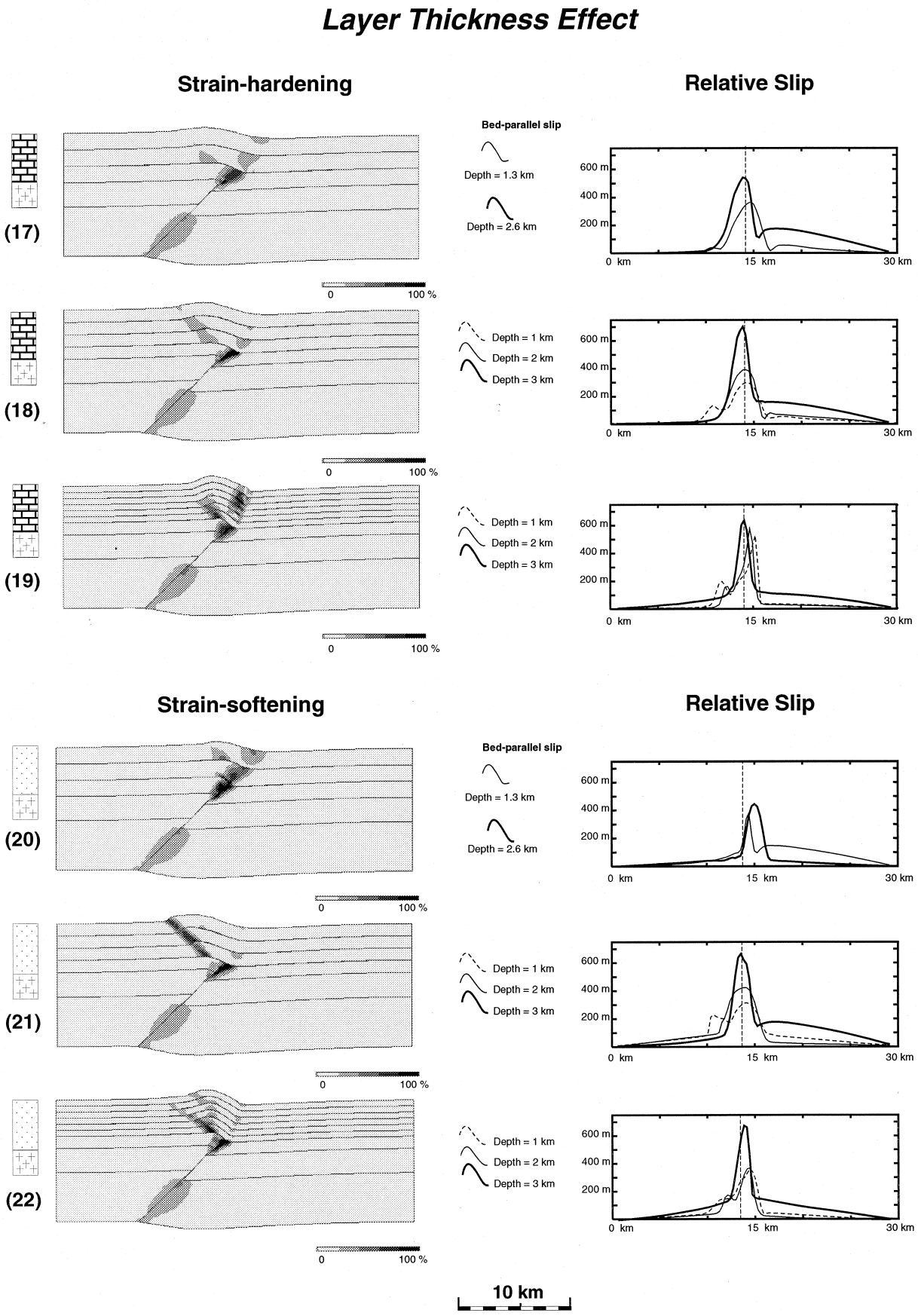

Fig. 8. Effect of the number of layers (thickness) on blind thrust propagation. Competing effects of faulting vs folding. In cases 17 and 20, faulting dominates with a rather straight propagation path. In cases 18 and 21, both backthrust faulting and folding are present. Lastly, cases 19 and 22 present the fold enhancement consequence of the great number of layers allowing bed-parallel slip.

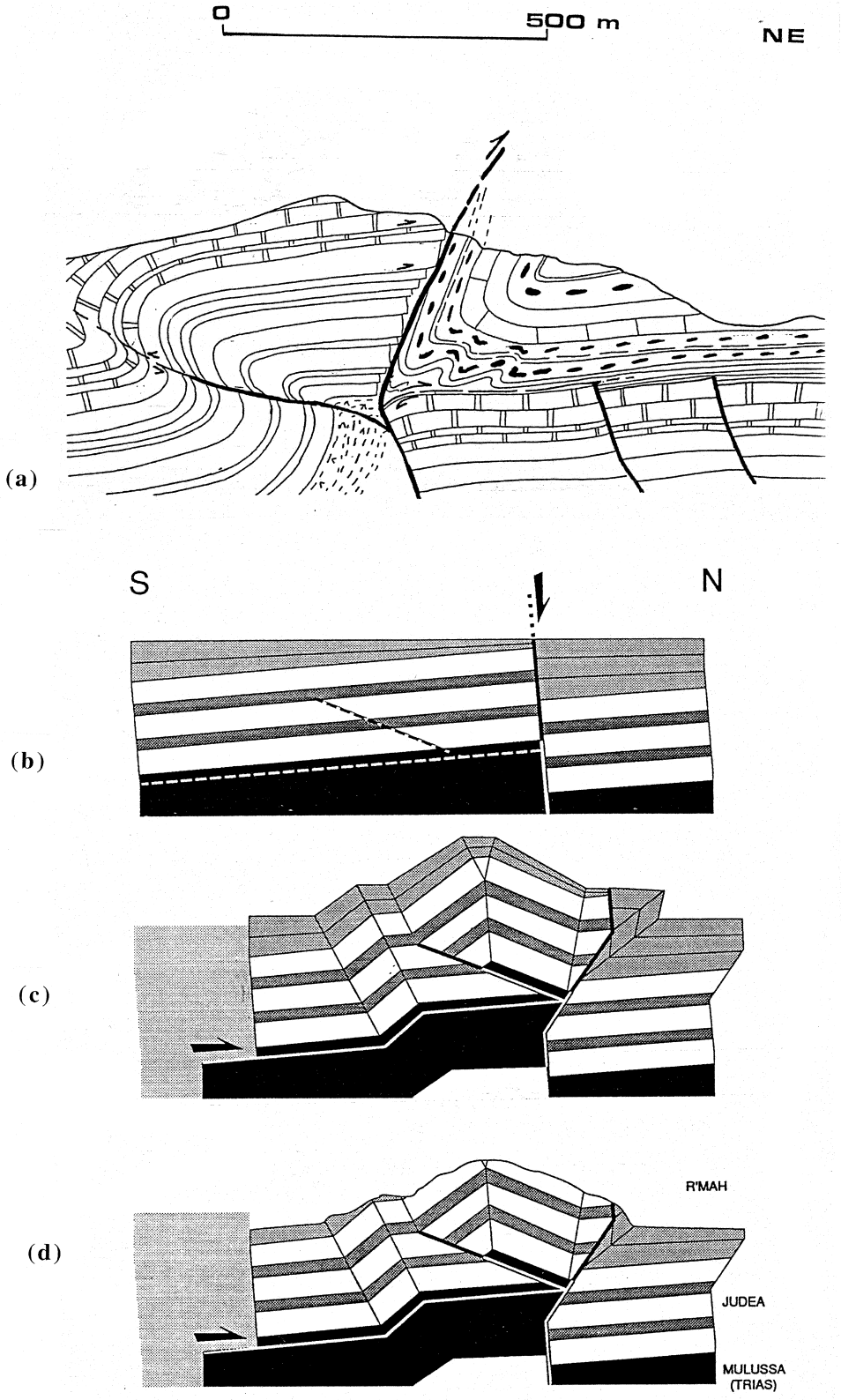

Fig. 9. (a) Cross-section along the Jabal Mquebra anticline in the Palmyrides (Syria). (b) and (c) Model of the evolution of Jabal Mquebra fault. (d) The final situation of the Jabal Mquebra fault, once erosion effects are considered. Balanced cross-sections from Salel (1993).

been used in our models: (1) the superficial layer of the model is completely flat before deformation; we have observed (these results have not been shown) that the presence of altitude variations at the surface can have an important influence on the fault propagation path. For simplicity, this effect has been neglected. (2) Layer thickness has been varied between 500 and 1333 m to study its effects. However, while sedimentary layers whose total thickness is of this order of magnitude are common in nature, relative slip takes place between stratigraphic units which are much thinner. Therefore, we have only considered slip between kilometric "macro-units", a situation which may represent that of a relatively thin layer (of salt, for example) enhancing slip between these macro-units. (3) When present, slip in our models exists between surfaces with a very small friction coefficient of $\mu = 0.05$, to exaggerate the consequences of this factor. Under these assumptions, we must underline the fact that the models considered represent cases that are not commonly found in nature, but that show important features that may be found in the field to a lesser extent. For instance, in the field most thrust faults are observed (or interpreted) to propagate forward; some of our models indicate a backthrust can be more active than the straight-path propagated fault, as is shown in the field example we present.

Given the hypotheses stated above, our models have shown four important features of blind thrust propagation through sedimentary layers: (1) Bed-parallel slip controls the final shape of the propagated fault in sedimentary layers, much more than rheology. This is true both for strain-softening and strain-hardening elastic–plastic rheologies, although the former enhances the effect of strain-localization. (2) Bed-parallel slip implies a mechanical decoupling between the sedimentary layers, which then act as guides for the transfer of stress. This stress-transfer mechanism extends the region of influence of the thrust fault, enabling deformation to go further than if it was not present. (3) With bed-parallel slip, high-angle thrust faults are shown preferentially split rather than form a backthrust, as is the general case. For mid- and low-angle faults, backthrusting remains an important mechanism for accommodating deformation. (4) Increasing the number of layers enhances the deformation-absorption effect of bed-parallel slip. Faulting and folding act on one another to increase fold amplitude and reduce the intensity of strain localization

If the rheology of sedimentary layers is known, the surface expression of deformation can be used to discriminate fault geometry at depth. More difficult to quantify is the amount of bed-parallel slip that a given sedimentary layer can accommodate. Furthermore, interpretation of natural folds is hindered by the accumulated effects of erosion, which have been neglected here. Nevertheless, the knowledge of the existence of these "backthrusting" and "fault splitting" effects can give new insights for the interpretation of recent tectonic features.

Acknowledgements—This is BRGM contribution number 96046. This work was financially supported by a BRGM research project. We are grateful for the invaluable technical help from R. Hassani and for the thoughtful comments of C. Teyssier. M. Jean (LMGC Montpellier) provided us his implementation of the contact-friction algorithm.

REFERENCES

Baidyuk, B. V. (1967) *Mechanical properties of rocks*. Consultants Bureau, New York.

Board, M. (1989) *FLAC (Fast Lagrangian Analysis of Continua) v2. 20: Software summary*. Itasca Consulting Group, Minneapolis.

Bray, J. D., Seed, R. B., Cluff, L. S. and Seed, H. B. (1994a) Earthquake fault rupture propagation through soil. *Journal of Geotechnical Engineering* **120,** 543–561.

Bray, J. D., Seed, R. B. and Seed, H. B. (1994b) Analysis of earthquake fault rupture propagation through cohesive soil. *Journal of Geotechnical Engineering* **120,** 562–580.

Caskey, S. J. (1995) Geometric relations of dip slip to a faulted ground surface: new nomograms for estimating components of fault displacement. *Journal of Structural Geology* **17,** 1197–1202.

Cole, D. A. and Lade, P. V. (1984) Influence zones in alluvium over dip-slip faults. *Journal of Geotechnical Engineering* **110,** 599–615.

Cundall, P. A. (1989) Numerical experiments on localization in frictional materials. *Ingenieur Archives* **58,** 148–159.

Duncan, J. M., Byrne, P., Wong, K. S. and Mabry, P. (1980) *Strength, stress–strain and bulk modulus parameters for finite-element analysis of stresses and movements in soil masses*. Rep. UCB/GT/80_01 University of California, Berkeley.

Hafner, W. (1951) Stress distributions and faulting. *Bulletin of the Geological Society of America* **62,** 373–398.

Handin, J. and Hager, R. (1957) Experimental deformation of sedimentary rocks under confining pressure tests at room temperature on dry samples. *Bulletin of the American Association of Petroleum Geologists* **41,** 1–50.

Hassani, R. (1994) *Modélisation numérique de la déformation des systèmes géologiques*. Ph. D. thesis, Université Montpellier II.

Huftile, G. J. and Yeats, R. S. (1996) Deformation rates across the Placerita (Northridge Mw = 6.7 aftershock zone) and Hopper Canyon segments of the Western Transverse Ranges deformation belt. *Bulletin of the Seismological Society of America* **86**(1B), S3–S18.

Johnson, A. M. (1980) Folding and faulting of strain-hardening sedimentary rocks. *Tectonophysics* **62,** 251–278.

Lade, P. V., Cole, D. A. and Cummings, D. (1984) Multiple failure surfaces over dip-slip faults. *Journal of Geotechnical Engineering* **110,** 616–627.

Lawn, B. R. (1993) *Fracture of brittle solids*. Cambridge University Press, Cambridge.

Lebel, D. and Mountjoy, E. Z. (1995) Numerical modeling of propagation and overlap of thrust faults, with application to the thrust-fold belt of central Alberta. *Journal of Structural Geology* **17,** 631–646.

Leroy, Y. and Ortiz, M. (1989) Finite element analysis of strain localization in frictional materials. *International Journal of Numerical Analysis Methods in Geomechanics* **13,** 53–74.

May, P. R. (1991) The eastern Mediterranean Mesozoic basin evolution and oil habitat. *AAPG Bulletin* **75,** 1215–1232.

Meissner, R. (1986) *The continental crust*. Academic Press. London.

Morse, J. (1977a) Deformation in the ramp regions of overthrust faults; experiments with small-scale, rock models. In *Rocky Mountain Thrust Belt; geology and resources*, eds E. L. Heisey, D. E. Lawson and E. R. Norwood, pp. 457–470. Wyoming Geological Association Guidebook, **29**.

Morse, J. (1977b) Experimental study of the deformation in ramp regions of overthrust faults (abstract). *EOS Transactions of the American Geophysical Union* **58,** 507.

Niño, F. (1996) *Modélisation numérique de la propagation de failles: localisation de la déformation*. Ph. D. thesis, Université Montpellier II.

O'Keefe, F. X. and Sengor, A. M. C. (1988) Tectonic Evolution of the Palmyra Zone Syria. *AAPG Bulletin (abstract)* **72,** 1017.
Patton, T. L. and Fletcher, R. C. (1995) Mathematical block-motion model for deformation of a layer above a buried fault of arbitrary dip and sense of slip. *Journal of Structural Geology* **17,** 1455–1472.
Philip, H. and Meghraoui, M. (1983) Structural analysis and interpretation of the surface deformation of the El Asnam earthquake of October 10, 1980. *Tectonics* **2,** 17–49.
Rodgers, D. A. and Rizer, W. D. (1981) Deformation and secondary faulting near the leading edge of a thrust fault. In *Thrust and nappe tectonics*, eds K. R. McClay and N. J. Price, pp. 65–77. Geological Society Special Publication, **9**.
Roering, J. J., Cooke, M. and Pollard, D. (1997) Why blind thrust faults don't propagate to the Earth's surface: numerical modeling of coseismic deformation associated with thrust-related anticlines. *Journal of Geophysical Research* **102**(B6), 11901–11912.
Rudnicki, J. W. and Rice, J. R. (1975) Conditions for the localization of deformation in pressure-sensitive materials. *Journal of the Mechanics and Physics of Solids* **23,** 371–394.
Salel, J. F. (1993) *Tectonique de chevauchement et inversion dans la chaine des Palmyrides et le graben de l'Euphrate (Syrie). Conséquence sur l'évolution de la plaque Arabe*. Ph. D. thesis, Université Montpellier II.
Sanford, A. R. (1959) Analytical and experimental study of simple geologic structures. *Geological Society of America Bulletin* **70,** 19–52.
Shaw, J. H. and Suppe, J. (1996) Earthquake hazards of active blind-thrust faults under the central Los Angeles basin, California. *Journal of Geophysical Research* **101**(B4), 8623–8642.
Suppe, J. (1983) Geometry and kinematics of fault-bend folding. *American Journal of Science* **283,** 684–721.
Touloukian, Y. S., Judd, W. R. and Roy, R. F. (1981) *Physical properties of rocks and minerals*. MacGraw-Hill, New York.
Walsh, J. J. and Watterson, J. (1988) Analysis of the relationship between displacements and dimensions of faults. *Journal of Structural Geology* **10,** 239–247.
Woodward, N. B., Boyer, S. E. and Suppe, J. (1989) *Balanced geological cross-sections: an essential technique in geological research and exploration*. American Geophysical Union.
Yeats, R. S. and Huftile, G. J. (1995) The Oak Ridge fault system and the 1994 Northridge earthquake. *Nature* **373,** 418–420.

APPENDIX

The general definition of an elastoplastic constitutive law implies the designation of a *yield stress* that is the boundary between two qualitatively different regimes: elastic (reversible deformation) and plastic (irreversible deformation). There exist many ways of defining the elastic behaviour of a material; for the sake of simplicity, we assume it follows Hooke's law of linear elasticity—we will be concerned only in the defining the post-yield or plastic behaviour. The yield stress is, in general, a function of the stress tensor σ and of a strain-softening/hardening parameter κ (that will represent the accumulated weakness of the material); it will be denoted by $F(\sigma,\kappa)$. The post-yield behaviour is defined by linking the deformation rate to a plastic potential, $G(\sigma,\kappa)$, by the relation:

$$\dot{\epsilon}_{ij} = \lambda_p \frac{\partial G(\sigma, \kappa)}{\partial \sigma_{ij}} \tag{A1}$$

where λ_p is a proportionality factor. Any plastic law is then fully determined when the yield function F and the plastic potential G are specified.

The elastoplastic constitutive law we use is Drucker–Prager's model, which is a function of both pressure and deviatoric stress.

It is fully defined if we establish the form of F, G and the parameter κ. The relations used are those proposed by Leroy and Ortiz (1989). The yield function is defined by:

$$F(\sigma, \kappa) = \sigma_{\text{eff}}(p, \text{dev}(\sigma), \kappa) - \sigma_{\text{Y}}(\kappa) = 0 \tag{A2}$$

where p is the pressure and dev(σ) the norm of the deviatoric stress tensor times $\sqrt{(3/2)}$; κ is the strain-hardening/weakening parameter, defined as the cumulative plastic deformation ($\dot{\epsilon}_{\text{p}}$ being the rate of plastic deformation):

$$\kappa(t) = \int_0^t \sqrt{\frac{2}{3}\dot{\epsilon}_{\text{p}} : \dot{\epsilon}_{\text{p}}}\, \text{d}\tau \tag{A3}$$

and

$$\sigma_{\text{eff}} = \text{dev}(\sigma) + \frac{p\alpha(\kappa)}{3} \tag{A4}$$

$$\sigma_{\text{Y}} = \alpha(\kappa) c \text{ cotan } \phi(\kappa) \tag{A5}$$

$$\alpha(\kappa) = \frac{6 \sin \phi(\kappa)}{3 - \sin \phi(\kappa)} \tag{A6}$$

where c is the cohesion and ϕ the angle of internal friction that depends on the parameter κ:

$$\sin \phi(\kappa) = \sin \phi_{\text{i}} + 2(\sin \phi_{\text{f}} - \sin \phi_{\text{i}}) \frac{\sqrt{\kappa_{\text{c}}\kappa}}{\kappa_{\text{c}} + \kappa} \tag{A7}$$

Thus, the angle of internal friction changes between an initial value ϕ_{i} and a final value ϕ_{f} reached after the cumulated deformation attains the value κ_{c}. If the final value of the friction angle is greater than the initial one, it is strain-hardening law; otherwise, it is a strain-softening one. The plastic potential is given by the function:

$$G(\sigma) = \text{dev}(\sigma) + \frac{2 \sin \psi}{2 - \sin \psi} p \tag{A8}$$

ψ being the dilatancy angle. Hence this law needs five plastic parameters: c (cohesion), ψ (dilatancy), ϕ_{i} and ϕ_{f} (initial and final friction angles), and the limiting value of the strain-softening/hardening parameter, κ_{c}.